JACS
JOURNAL OF THE AMERICAN CHEMICAL SOCIETY
Communication
pubs.acs.org/JACS

Femtosecond Time-Resolved Transient Absorption Spectroscopy of $CH_3NH_3PbI_3$ Perovskite Films: Evidence for Passivation Effect of PbI_2

Lili Wang,[†] Christopher McCleese,[†] Anton Kovalsky,[†] Yixin Zhao,*[,‡] and Clemens Burda*[,†]

[†]Department of Chemistry, Case Western Reserve University, 10900 Euclid Avenue, Cleveland, Ohio 44106, United States
[‡]School of Environmental Science and Engineering, Shanghai Jiao Tong University, 800 Dongchuan Road, Shanghai 200240, China

Supporting Information

ABSTRACT: $CH_3NH_3PbI_3$ perovskite layered films deposited on substrates with and without a titania support structure have been prepared and studied using time-resolved femtosecond transient absorption (fs-TA) spectroscopy in the visible light range (450−800 nm). The electron injection dynamics from the photoexcited perovskite layers to the neighboring film structures could be directly monitored via the transient bleaching dynamics of the perovskite at ∼750 nm and thus systematically studied as a function of the layer-by-layer architecture. In addition, for the first time we could spectrally distinguish transient bleaching at ∼750 nm from laser-induced fluorescence that occurs red-shifted at ∼780 nm. We show that an additional bleach feature at ∼510 nm appears when PbI_2 is present in the perovskite film. The amplitudes of the PbI_2 and perovskite TA peaks were compared to estimate relative amounts of PbI_2 in the samples. Kinetic analysis reveals that perovskite films with less PbI_2 show faster relaxation rates than those containing more PbI_2. These fast dynamics are attributed to charge carrier trapping at perovskite grain boundaries, and the slower dynamics in samples containing PbI_2 are due to a passivation effect, in line with other recently reported work.

Organic/inorganic trihalide lead-based perovskites have attracted much attention worldwide because solar cell devices fabricated with this group of materials have demonstrated high power conversion efficiency (PCE).[1−5] Since the introduction of lead halide perovskite sensitized solar cells,[6,7] many groups have contributed to improving their performance and stability.[8−14] Despite the tremendous progress, many questions remain as to why certain architectures perform better than others.

Two main architectures are considered for solid-state perovskite-based solar cells: planar[13] and mesoporous[10] structures. The different layers in both structures affect the separation, transport, and recombination kinetics of the photoinduced charge carriers. According to Hodes et al., a mesoporous electron conductor is necessary to optimize $CH_3NH_3PbI_3$-based solar cell devices with high PCE.[15] The mesoporous layer is usually fabricated with titanium oxide (TiO_2)[11] or aluminum oxide (Al_2O_3)[10] nanoparticles. Snaith's group reported perovskite solar cells with higher open-circuit voltage (V_{oc}) by employing mesoporous Al_2O_3 (V_{oc} = 0.98 eV) instead of TiO_2 (V_{oc} = 0.8).[10] The PCE of planar $CH_3NH_3PbI_3$-based solar cells without mesoporous TiO_2 has been reported to reach 13.7%.[16] The role of mesoporous TiO_2 is complicated.

Scheme 1. Architectures Studied in This Work

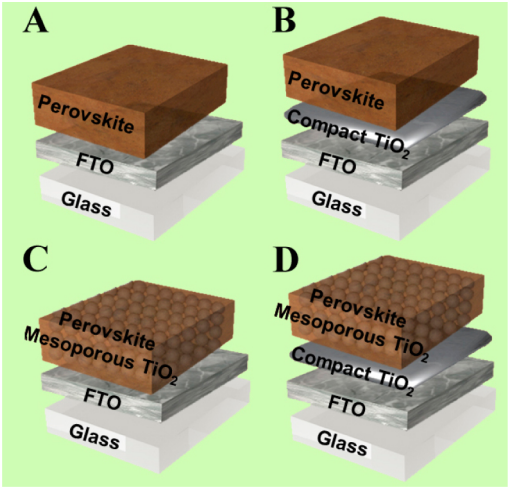

Previous studies revealed that PbI_2 would form due to decomposition of the lead halide perovskite.[17−19] Dittrich et al. showed that, depending on the sintering temperature, PbI_2 can form in perovskite films. Their work showed that, under certain conditions, PbI_2 can act as a passivation layer or defect states can form at the perovskite/PbI_2 interface.[18] Recently, Yang et al. also showed that PbI_2 can fill perovskite grain boundaries, thereby reducing the number of trapping sites and also allowing for a more favorable band bending.[20] This led to slower charge carrier recombination times and enhanced PCE in perovskite films containing PbI_2. The band edges of PbI_2 are offset such that they form a type-I interface with perovskites. If too much PbI_2 is present it could act as an insulating layer rather than a passivation layer. Thus, it is important to understand the role of PbI_2 on the dynamics of photoexcited perovskite films.

Although there have been some time-resolved femtosecond transient absorption (fs-TA) studies, few have probed within the visible spectrum,[8,21,22] because the samples studied contained a hole-transport material (HTM), such as spiro-OMeTAD. The addition of a HTM causes the visible spectrum to become optically dense, possibly necessitating probing outside the visible light range. This was recently accomplished by Moser et al.[23] to

Received: May 8, 2014
Published: August 22, 2014

   dx.doi.org/10.1021/ja504632z | J. Am. Chem. Soc. 2014, 136, 12205−12208

evaluate the lifetimes of excited electrons at 1.4 μm probe wavelength. Sundström et al.[24] also measured the formation and lifetime of mobile electrons at 970 nm.

In this work, we present fs-TA laser pump/probe spectroscopy as a unique tool for identifying the formation of PbI_2 impurities with much greater clarity than steady-state visible light absorption spectroscopy. One can use fs-TA spectra to quantify the relative amount of PbI_2 in perovskites, while powder X-ray diffraction (XRD) can independently confirm the presence of PbI_2. We go on to further study the systematically altered architectures deposited on fluorine-doped tin oxide (FTO) glass by measuring the charge carrier dynamics of the samples at the perovskite band edge. Combined structural and kinetic analysis of these interfaces provides insight into the charge carrier dynamics of $CH_3NH_3PbI_3$ perovskites in their particular chemical and structural environment.

The compact TiO_2,[6] mesoporous TiO_2,[25] and perovskite films[26] were prepared by following previous reports. The resulting architectures are summarized in Scheme 1. The samples were characterized and measured immediately after fabrication.

Figure 1 shows the XRD characterization of samples in this work. We find that the impurity peaks around 12.5° and 25.8°

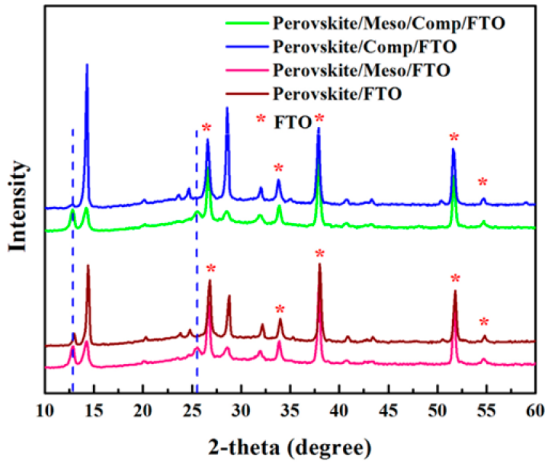

Figure 1. X-ray diffraction patterns of the various perovskite film architectures showing varying amounts of PbI_2 (blue dashed lines) within the prepared perovskite samples. Peaks from the FTO substrate are also observed (asterisks).

(blue dashed line) can be attributed to PbI_2 crystals in these samples. The presence of PbI_2 is more pronounced in samples with a mesoporous TiO_2 layer. The diffraction peaks assigned to the perovskite demonstrate additional broadening in samples with a mesoporous TiO_2 layer compared to the ones without a mesoporous layer. Rietveld analysis indicates that mesoporous TiO_2 leads to smaller grain sizes (Table 1) in perovskite, which is in accordance with SEM observations reported previously.[17] As expected, one also finds FTO peaks (JCPDS 77-0447), denoted in Figure 1with asterisks.

Our fs-TA setup is composed of a Ti:sapphire laser (Clark MXR 2001) that outputs 120 fs pulses of 780 nm wavelength at 1 kHz repetition rate. The 780 nm beam is split, sending one part to a sapphire crystal to generate a white light continuum of 450–800 nm and the other part to a second harmonic generating crystal to produce a 390 nm pump beam or to an optical parametric amplifier (Light Conversion Ltd.) for visible pump wavelengths (450–750 nm).

Table 1. Mean Grain Sizes of Perovskite and PbI_2 Determined by Rietveld Analysis

		mean grain size/nm	
sample[a]	abbreviation[b]	perovskite	PbI_2
A	perovskite/FTO	33	29
B	perovskite/comp/FTO	43	19
C	perovskite/meso/FTO	16	20
D	perovskite/meso/comp/FTO	16	20

[a]Letters A–D correspond to the labels in Scheme 1. [b]comp = compact TiO_2; meso = mesoporous TiO_2.

Figure 2 shows the normalized ground-state absorption, normalized photoluminescence (PL) spectra (top panels), and

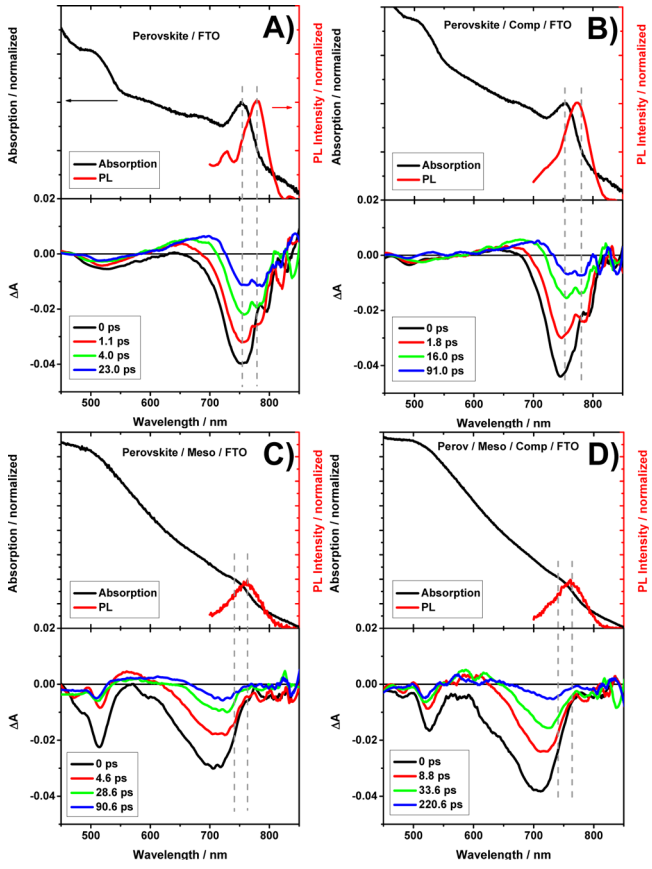

Figure 2. Normalized ground-state absorption, PL (top panels), and fs-TA spectra at various time delays after photoexcitation (bottom panels) of the fabricated architectures (A–D, refer to Scheme 1). The gray dashed lines are a guide for indicating the band edge absorption and PL peak positions.

fs-TA spectra (bottom panels) of the samples introduced in Scheme 1. From the TA spectra of perovskite/FTO and perovskite/comp/FTO (Figure 2A,B), there are four main features: a photoinduced transient bleach at ~500 nm, a photoinduced TA in the range of 600–700 nm, a second bleach signal at ~750 nm, and an additional transient signal at ~780 nm. The features at 750 and 780 nm can be assigned to transient bleaching of the band edge transition and laser-induced fluorescence by comparison with the steady-state absorption and PL spectra, respectively. Upon coating perovskite on mesoporous TiO_2 (Figure 2C,D), we find different spectroscopic features compared to perovskite/FTO (A) and perovskite/

dx.doi.org/10.1021/ja504632z | J. Am. Chem. Soc. 2014, 136, 12205–12208

comp/FTO (B). First, looking at the UV/vis absorption spectrum, the band edge absorption peak is not as well defined as for perovskite/FTO or perovskite/comp/FTO in Figure 2A,B. It has been reported that perovskite can form nanograins when coated on mesoporous TiO_2.[7] A wide size distribution of the formed nanograins could lead to the observed broadening of the absorption spectra and would have other photophysical implications, such as energy transfer from smaller to larger particles upon excitation.[27] This broadening is observed in the fs-TA spectra as well. Another difference is that the transient band edge bleach is blue-shifted for perovskite deposited on mesoporous TiO_2 compared to that on planar structures. This blue shift can be attributed to different grain sizes in these samples (Table 1). In forming nanograins, compared to films, the quantum confinement in the photoexcited nanograins is greater.

The XRD results in Figure 1, along with the XRD of pure PbI_2 in Figure S1 of the Supporting Information, show that PbI_2 forms in samples supported on mesoporous TiO_2. PbI_2 has a bulk band gap of 2.3 eV,[18] commensurate with the highest energy bleach in our fs-TA spectra. TA spectra of pure PbI_2 are shown in Figure S2 for comparison. fs-TA measurements exciting at 390 and 600 nm of PbI_2-rich samples are provided in Figure S3 to show how excitation wavelength affects the TA spectra.

Samples show variations in the TA peak intensities when comparing the PbI_2 bleach at ~510 nm and the perovskite band edge bleach on planar and mesoporous structures. The peak intensities were used to determine the relative amounts of PbI_2 present in the samples (Table 2). We find that perovskite/FTO

Table 2. Ratio of Bleach Intensities at ~510 nm and at the Band Edge for Samples A–D

architecture	bleach ratio (PbI_2:perovskite)
perovskite/FTO	1:7
perovskite/comp/FTO	1:13
perovskite/meso/FTO	1:1.3
perovskite/meso/comp/FTO	1:2.3

(A) and perovskite/comp/FTO (B) show minimum amounts of PbI_2, with PbI_2-to-perovskite ratios of 1:7 and 1:13, respectively. However, perovskite/meso/FTO (C) and perovskite/meso/comp/FTO (D) show higher amounts of PbI_2, with ratios of 1:1.3 and 1:2.3, respectively. This peak ratio analysis shows that the morphology of the substrate plays a significant role in the crystallization process and stability of perovskites. This was also shown in Figure 3 of ref 17.

To study the relaxation dynamics, the decay kinetics of the related band edge bleaching were measured (Figure 3), and the obtained kinetic fits are summarized in Table 3. To investigate if multiple excitations could complicate the relaxation dynamics, a pump power dependence study was performed and is presented in Figure S4. It was found that decreasing pump fluence did not slow down the relaxation dynamics, confirming that no multiple-excitation effects were detectable here.

The fit of the kinetics for perovskite/FTO at 748 nm showed two time constants, 2.2 ps (55%) and 39.0 ps (45%). The fast component for this sample is attributed to charge carrier trapping at perovskite grain boundaries. Based on the XRD results and the fs-TA peak ratio analysis, very little PbI_2 is present in this sample. Thus, there should be many unfilled grain boundaries within the perovskite film that can act as charge carrier recombination centers. Although some of the carriers become trapped, it is expected that there is still charge carrier transfer between

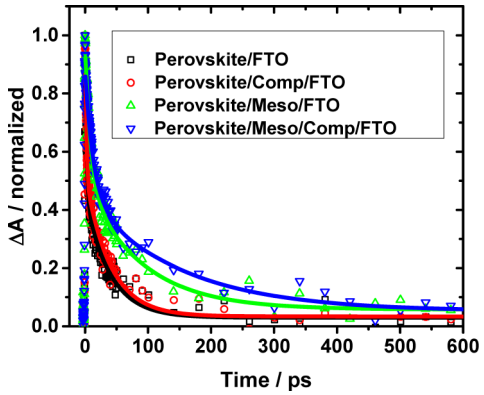

Figure 3. Transient band edge bleach kinetics (symbols) and their fits (lines) for perovskite architectures A–D at probe wavelengths λ_{probe} as noted in Table 3.

Table 3. Kinetic Fit Parameters for Perovskite Architectures

architecture	λ_{probe}/nm	τ_1/ps	τ_2/ps
perovskite/FTO	748	2.2 ± 0.2 (55%)	39.0 ± 2.8 (45%)
perov/comp/FTO	750	1.7 ± 0.1 (51%)	39.9 ± 2.5 (49%)
perov/meso/FTO	728	9.1 ± 0.8 (52%)	89.6 ± 12.5 (48%)
perov/meso/comp/FTO	722	13.5 ± 1.0 (52%)	150.0 ± 17.6 (48%)

photoexcited perovskite and FTO. Thus, we assign the longer time component (τ_2) to electron injection into FTO. There is a third component in the kinetic trace that does not decay within the instrument-limited 3 ns time window. This long-lifetime component, not resolved in this work, is most likely electron–hole recombination.[20,21,23,24,28,29] This conclusion is further supported by time-resolved PL measurements shown in Figure S5.

The idea of introducing a compact TiO_2 layer is to have efficient electron injection into FTO while slowing the rate of back electron transfer to perovskite. From the fit of the kinetics for perovskite/comp/FTO, time constants of 1.7 ps (50%) and 39.0 ps (48%) are obtained. This indicates that the additional presence of a compact TiO_2 layer does not hinder electron injection from perovskite to FTO.

The fit of the kinetics for perovskite/meso/FTO (C) shows slower time constants of 9.1 ps (52%) and 89.6 ps (48%) compared to perovskite/FTO (A) and perovskite/comp/FTO (B). Different from the perovskite/FTO and perovskite/comp/FTO samples, it is clear that the morphological changes on mesoporous TiO_2 alter the transport and relaxation properties. From the XRD results and fs-TA bleach ratio analysis above, mesoporous TiO_2 facilitates the formation of PbI_2. Dittrich showed that, at higher sintering temperatures, PbI_2 could possibly lead to interfacial defect states that can act as charge carrier trapping centers.[18] Under our synthesis conditions, it is more likely that PbI_2 forms as a passivating layer which leads to longer recombination times. The longer time constants observed for the samples containing a mesoporous substrate indicate that passivation through PbI_2 has occurred. Similar time constants are found for perovskite/meso/comp/FTO (D), 13.5 ps (52%) and 150 ps (48%).

In summary, fs-TA spectroscopy probed in the visible spectrum, when coupled with XRD, is a useful tool for determining the relative amounts of PbI_2 and its effect on the relaxation kinetics within photovoltaic perovskite structures. We

dx.doi.org/10.1021/ja504632z | J. Am. Chem. Soc. 2014, 136, 12205–12208

find that mesoporous TiO_2 is more likely to induce the formation of PbI_2 than compact TiO_2. This leads to the passivation of perovskite grain boundaries. Our work shows that injection rates are slowed in the presence of more PbI_2. Recent work has shown that carrier recombination lifetimes are also slowed upon passivation.[20] It will require extensive work to determine the optimum amount of PbI_2 for the best passivation to eliminate defect states. Interestingly, PbI_2 is a commonly observed byproduct in the aging process of perovskite solar cells. Thus, identifying, quantifying, and studying the effects of PbI_2 formation is necessary for improving future perovskite-based solar cells. The presented fs-TA analysis may play a useful role in this process.

■ ASSOCIATED CONTENT

Supporting Information

XRD, absorption, PL, and fs-TA spectra of pure PbI_2; fs-TA and TR-PL of perovskite excited at 600 nm; and pump power dependence. This material is available free of charge via the Internet at http://pubs.acs.org.

■ AUTHOR INFORMATION

Corresponding Authors

yixin.zhao@sjtu.edu.cn
burda@case.edu

Notes

The authors declare no competing financial interest.

■ ACKNOWLEDGMENTS

C.B. thanks Charles Kolodziej for help with film deposition. Y.Z. gratefully acknowledge the National Natural Science Foundation of China (Grant No. 51372151) for financial support.

■ REFERENCES

(1) Hodes, G. *Science* **2013**, *342*, 317.
(2) Snaith, H. J. *J. Phys. Chem. Lett.* **2013**, *4*, 3623.
(3) Park, N.-G. *J. Phys. Chem. Lett.* **2013**, *4*, 2423.
(4) Kamat, P. V. *J. Am. Chem. Soc.* **2014**, *136*, 3713.
(5) Kazim, S.; Nazeeruddin, M. K.; Grätzel, M.; Ahmad, S. *Angew. Chem., Int. Ed.* **2014**, *53*, 2812.
(6) Kojima, A.; Teshima, K.; Shirai, Y.; Miyasaka, T. *J. Am. Chem. Soc.* **2009**, *131*, 6050.
(7) Im, J. H.; Lee, C. R.; Lee, J. W.; Park, S. W.; Park, N. G. *Nanoscale* **2011**, *3*, 4088.
(8) Kim, H. S.; Lee, C. R.; Im, J. H.; Lee, K. B.; Moehl, T.; Marchioro, A.; Moon, S. J.; Humphry-Baker, R.; Yum, J. H.; Moser, J. E.; Grätzel, M.; Park, N. G. *Sci. Rep.* **2012**, *2*, 591.
(9) Etgar, L.; Gao, P.; Xue, Z.; Peng, Q.; Chandiran, A. K.; Liu, B.; Nazeeruddin, M. K.; Grätzel, M. *J. Am. Chem. Soc.* **2012**, *134*, 17396.
(10) Lee, M. M.; Teuscher, J.; Miyasaka, T.; Murakami, T. N.; Snaith, H. J. *Science* **2012**, *338*, 643.
(11) Burschka, J.; Pellet, N.; Moon, S. J.; Humphry-Baker, R.; Gao, P.; Nazeeruddin, M. K.; Grätzel, M. *Nature* **2013**, *499*, 316.
(12) Zhang, W.; Saliba, M.; Stranks, S. D.; Sun, Y.; Shi, X.; Wiesner, U.; Snaith, H. J. *Nano Lett.* **2013**, *13*, 4505.
(13) Liu, M.; Johnston, M. B.; Snaith, H. J. *Nature* **2013**, *501*, 395.
(14) Christians, J. a; Fung, R. C. M.; Kamat, P. V. *J. Am. Chem. Soc.* **2014**, *136*, 758.
(15) Edri, E.; Kirmayer, S.; Henning, A.; Mukhopadhyay, S.; Gartsman, K.; Rosenwaks, Y.; Hodes, G.; Cahen, D. *Nano Lett.* **2014**, *14*, 1000.
(16) Yella, A.; Heiniger, L. P.; Gao, P.; Nazeeruddin, M. K.; Grätzel, M. *Nano Lett.* **2014**, *14*, 2591.
(17) Zhao, Y.; Zhu, K. *J. Phys. Chem. C* **2014**, *118*, 9412.
(18) Supasai, T.; Rujisamphan, N.; Ullrich, K.; Chemseddine, A.; Dittrich, T. *Appl. Phys. Lett.* **2013**, *103*, No. 183906.
(19) Dualeh, A.; Tétreault, N.; Moehl, T.; Gao, P.; Nazeeruddin, M. K.; Gratzel, M. *Adv. Funct. Mater.* **2014**, *24*, 3250.
(20) Chen, Q.; Zhou, H.; Song, T.-B.; Luo, S.; Hong, Z.; Duan, H.-S.; Dou, L.; Liu, Y.; Yang, Y. *Nano Lett.* **2014**, *14*, 4158.
(21) Zhu, Z.; Ma, J.; Wang, Z.; Mu, C.; Fan, Z.; Du, L.; Bai, Y.; Fan, L.; Yan, H.; Phillips, D. L.; Yang, S. *J. Am. Chem. Soc.* **2014**, *136*, 3760.
(22) Xing, G.; Mathews, N.; Sun, S.; Lim, S. S.; Lam, Y. M.; Grätzel, M.; Mhaisalkar, S.; Sum, T. C. *Science* **2013**, *342*, 344.
(23) Marchioro, A.; Teuscher, J.; Friedrich, D.; Kunst, M.; van de Krol, R.; Moehl, T.; Grätzel, M.; Moser, J.-E. *Nat. Photonics* **2014**, *8*, 250.
(24) Ponseca, C. S.; Savenije, T. J.; Abdellah, M.; Zheng, K.; Yartsev, A.; Pascher, T.; Harlang, T.; Chabera, P.; Pullerits, T.; Stepanov, A.; Wolf, J.-P.; Sundström, V. *J. Am. Chem. Soc.* **2014**, *136*, 5189.
(25) Leijtens, T.; Lauber, B.; Eperon, G. E.; Stranks, S. D.; Snaith, H. J. *J. Phys. Chem. Lett.* **2014**, *5*, 1096.
(26) Zhao, Y.; Zhu, K. *J. Phys. Chem. Lett.* **2013**, *4*, 2880.
(27) Kagan, C. R.; Murray, C. B.; Nirmal, M.; Bawendi, M. G. *Phys. Rev. Lett.* **1996**, *76*, 1517.
(28) Stranks, S. D.; Eperon, G. E.; Grancini, G.; Menelaou, C.; Alcocer, M. J. P.; Leijtens, T.; Herz, L. M.; Petrozza, A.; Snaith, H. J. *Science* **2013**, *342*, 341.
(29) Xing, G.; Mathews, N.; Sun, S.; Lim, S. S.; Lam, Y. M.; Grätzel, M.; Mhaisalkar, S.; Sum, T. C. *Science* **2013**, *342*, 344.